

Photoproduction of $\Theta^+(1540, 1/2^+)$ reexamined with new theoretical information

Seung-il Nam^{1,*} and Hyun-Chul Kim^{2,†}

¹*Yukawa Institute for Theoretical Physics (YITP),
Kyoto University, Kyoto 606-8502, Japan*

²*Department of Physics, Inha University, Incheon 402-751, Korea.*

(Dated: May 29, 2022)

Abstract

We reinvestigate the photoproduction of the exotic pentaquark baryon $\Theta^+(1540, 1/2^+)$ from the $\gamma N \rightarrow \bar{K}\Theta^+$ reaction process within the effective Lagrangian approach, taking into account new theoretical information on the $KN\Theta$ and $K^*N\Theta$ coupling strengths from the chiral quark-soliton model (χ QSM). We also consider the crossing-symmetric hadronic form factor, satisfying the on-shell condition as well. Due to the sizable vector and tensor couplings for the vector kaon, $g_{K^*N\Theta}$ and $f_{K^*N\Theta}$, which are almost the same with the vector coupling $g_{KN\Theta} \approx 0.8$ for the pseudoscalar kaon, the K^* -exchange contribution plays a critical role in the photon beam asymmetries.

PACS numbers: 13.60.Le, 14.20.Jn

Keywords: Exotic pentaquark baryon, Θ^+ photoproduction

arXiv:0901.0771v1 [hep-ph] 7 Jan 2009

*E-mail: sinam@yukawa.kyoto-u.ac.jp

†E-mail: hchkim@inha.ac.kr

I. INTRODUCTION

Since the LEPS collaboration announced the evidence of the Θ^+ [1], being motivated by Ref. [2] in which its decay width was predicted to be very small with its mass 1540 MeV [3], it intrigued a great deal of experimental and theoretical works on the Θ^+ (see, for example, reviews [5, 6] for the experimental and theoretical status before 2006). However, the CLAS collaboration conducted a series of experiments and reported eventually null results of finding the Θ^+ [7, 8, 9, 10] in various reactions. Considering the fact that these CLAS experiments were dedicated ones with high statistics, these null results from the CLAS experiment are remarkable and indicate that the total cross sections for photoproductions of the Θ^+ should be tiny. In fact, the 95% confidence level (CL) upper limits on the total cross sections for the Θ^+ at 1540 MeV lie mostly in the range of (0.3 – 0.8) nb [7, 8, 10]. In Ref. [9] the upper limit on the $\gamma d \rightarrow \Lambda(1520, 3/2^-)\Theta^+$ total cross section turned out to be about 5 nb in the mass range from 1520 MeV to 1560 MeV with a 95 % CL. The KEK-PS-E522 collaboration [11] has carried out the experiment searching for the Θ^+ via the $\pi^- p \rightarrow K^- X$ reaction and found a bump at around 1530 MeV but with only (2.5 ~ 2.7) σ statistical significance. Moreover, the upper limit of the Θ^+ -production cross section in the $\pi^- p \rightarrow K^- \Theta^+$ reaction was extracted to be 3.9 μb . A later experiment at KEK (KEK-PS-E559), however, has observed no clear peak structure for the Θ^+ in the $K^+ p \rightarrow \pi^+ X$ reaction [12], giving a 95 % CL upper limit of 3.5 $\mu\text{b}/\text{sr}$ for the differential cross section averaged over from 2° to 22° in the laboratory system. This negative situation is summarized in the 2008 Review of Particle Physics by Wohl [4]: “*The whole story – the discoveries themselves, the tidal wave of papers by theorists and phenomenologists that followed, and the eventual “undiscovery” – is a curious episode in the history of science.*”

In the meanwhile, the DIANA collaboration has continued to search for the Θ^+ in the $K^+ n \rightarrow K^0 p$ reaction and has reported a direct formation of a narrow pK^0 peak with mass of (1537 ± 2) MeV and width of $\Gamma = (0.36 \pm 0.11)$ MeV [13]. Compared to the former measurement by the DIANA collaboration for the Θ^+ , the decay width was more precisely measured in this new experiment [14], the statistics being doubled. The SVD experiment has also reported a narrow peak with the mass, $(1523 \pm 2_{\text{stat.}} \pm 3_{\text{syst.}})$ MeV in the inclusive reaction $pA \rightarrow pK_s^0 + X$ [15, 16]. Moreover, the LEPS collaboration has brought news very recently on the evidence of the Θ^+ [17]: The mass of the Θ^+ is found at $(1525 \pm 2 + 3)$ MeV and the statistical significance of the peak turns out to be 5.1σ . The peak position is shifted by +3 MeV systematically due to the minimum momentum spectator approximation (MMSA). The differential cross section was estimated to be (12 ± 2) nb/sr in the photon energy ranging from 2.0 GeV to 2.4 GeV in the LEPS angular range.

Although it seems that the pentaquark baryon Θ^+ rarely exists according to certain experiments as explained above, it is still theoretically necessary to understand why the Θ^+ is so elusive and intractable. As mentioned previously, one of the reasons can be found in the fact that the cross sections of the Θ^+ photoproduction as well as of the mesonic production are observed to be minuscule. The origin of these tiny cross sections can be understood by the smallness of the $KN\Theta$ and $K^*N\Theta$ coupling constants, as mentioned explicitly in Refs. [12]. A similar conclusion was also found in Ref. [17]. Moreover, the decay width of the $\Theta^+ \rightarrow KN$, observed by the DIANA collaboration, indicates that the $KN\Theta$ coupling constant must be small, as was reviewed in Ref. [18]. From the theoretical side, Ref. [19] has shown that the tensor coupling constant for the $K^*N\Theta$ vertex is very small and has predicted the total cross section for the Θ^+ photoproduction to be around 0.2 nb even before the CLAS

measurement, in which the cross section for the Θ^+ photoproduction was estimated to be below (0.3 \sim 0.8) nb [7, 8, 10]. Azimov *et al.* [20] has evaluated the smaller value of the $K^*N\Theta$ tensor coupling constant, employing the vector meson dominance with SU(3) symmetry. The vector coupling constant for the $K^*N\Theta$ vertex vanishes in SU(3) symmetry due to the generalized Ademollo-Gatto theorem as shown in Ref. [21], in which the vector and tensor coupling constants for the $K^*N\Theta$ vertex turned out to be very small within the framework of the chiral quark-soliton model (χ QSM) with SU(3) symmetry breaking effects taken into account: The vector coupling constant $g_{K^*N\Theta} = 0.74 \sim 0.87$ and tensor coupling constant $f_{K^*N\Theta} = 0.53 \sim 1.16$, respectively. In the same theoretical framework, the $KN\Theta$ coupling constant was determined to be $g_{KN\Theta} = 0.83$, which leads to the corresponding the decay width of the Θ^+ : $\Gamma_{\Theta \rightarrow NK} = 0.71$ MeV [22]. Note that these results in the χ QSM are all derived without adjusting any parameters.

In Refs. [24, 25, 26, 29], the photoproduction of the Θ^+ was investigated, based on effective Lagrangian approaches. However, since the coupling constants and cut-off masses were unknown both experimentally and theoretically, it was very difficult to describe the production mechanism of the Θ^+ without any ambiguity. Thus, in the present work, we want to reexamine the photoproduction of the Θ^+ , incorporating the $KN\Theta$ and $K^*N\Theta$ coupling constants and cut-off masses from Refs. [21, 22]. The results will be shown that the magnitudes of the total cross section and differential cross section are qualitatively compatible with those of the LEPS and CLAS data.

We sketch the structure of the present work as follows: In Section II, we briefly review the coupling constants of the K and K^* exchange, which play critical roles in describing the photoproduction of the Θ^+ . In Section III, we explain the general formalism of the effective Lagrangian method. In Section IV, we present the numerical results and discuss them. The final Section is devoted to summary and conclusion.

II. COUPLING CONSTANTS AND FORM FACTORS FOR THE K AND K^* EXCHANGES FROM THE χ QSM

In this Section, we briefly review the results of the χ QSM calculations. We start with the following Θ^+ -to-neutron transition matrix elements of the vector current $V^\mu = \bar{\psi}\gamma^\mu\frac{1}{2}(\lambda^4 - i\lambda^5)\psi$, and axial-vector current $A^\mu = \bar{\psi}\gamma^\mu\gamma^5\frac{1}{2}(\lambda^4 - i\lambda^5)\psi$:

$$\langle\Theta(p')|V^\mu(0)|n(p)\rangle = \bar{u}_\Theta(\mathbf{p}') \left[F_1^{n\Theta}(Q^2)\gamma^\mu + \frac{F_2^{n\Theta}(Q^2)i\sigma^{\mu\nu}q_\nu}{M_\Theta + M_n} + \frac{F_3^{n\Theta}(Q^2)q^\mu}{M_\Theta + M_n} \right] u_n(\mathbf{p}) , \quad (1)$$

$$\langle\Theta(p')|A^\mu(0)|n(p)\rangle = \bar{u}_\Theta(\mathbf{p}') [G_1^{n\Theta}(Q^2)\gamma^\mu + G_2^{n\Theta}(Q^2)q^\mu + G_3^{n\Theta}(Q^2)P^\mu] \gamma^5 u_n(\mathbf{p}) , \quad (2)$$

where $u_{\Theta(n)}$ denotes the spinor of the Θ^+ (neutron) with the corresponding mass $M_{\Theta(n)}$. The Q^2 stands for the momentum transfer $Q^2 = -q^2 = -(p' - p)^2$ and P represents the total momentum $P = p' + p$. $F_i^{n\Theta}$ and $G_i^{n\Theta}$ designate real transition form factors, related to the strong coupling constants for the K^* and K with the help of the vector-meson dominance (VMD) [31, 32] and Goldberger-Treiman relations.

In the VMD, the vector-transition current can be expressed as the K^* current by the current field identity (CFI):

$$V^\mu(x) = \bar{s}(x)\gamma^\mu u(x) = \frac{m_{K^*}^2}{f_{K^*}} K^{*\mu}(x) , \quad (3)$$

where m_{K^*} and f_{K^*} denote, respectively, the mass of the K^* meson, $m_{K^*} = 892$ MeV, and decay constant defined as

$$f_{K^*}^2 = \frac{m_{K^*}^2}{m_\rho^2} f_\rho^2, \quad (4)$$

where the decay constant f_ρ for the rho meson can be determined as

$$f_\rho^2 = \frac{4\pi\alpha^2 m_\rho}{3\Gamma_{\rho^0 \rightarrow e^+e^-}}. \quad (5)$$

Here, α denotes the electromagnetic fine-structure constant. The f_{K^*} is determined by using the ρ -meson experimental data with $m_\rho = 770$ MeV and $\Gamma_{\rho^0 \rightarrow e^+e^-} = (7.02 \pm 0.11)$ keV [4], for which we get the values $f_\rho \approx 4.96$ and $f_{K^*} \approx 5.71$. Then, using the CFI, we can express the $K^*N\Theta$ vertex in terms of the transition form factors in Eqs. (1) and (2):

$$\langle \Theta(p') | \bar{s}\gamma^\mu u | n(p) \rangle = \frac{m_{K^*}^2}{f_{K^*}} \frac{1}{m_{K^*}^2 - q^2} \langle \Theta(p') | K^{*\mu} | n(p) \rangle, \quad (6)$$

$$\langle \Theta(p') | K^{*\mu} | n(p) \rangle = \bar{u}_\Theta(\mathbf{p}') \left[g_{K^*n\Theta} \gamma^\mu + f_{K^*n\Theta} \frac{i\sigma^{\mu\nu} q_\nu}{M_\Theta + M_n} + \frac{s_{K^*n\Theta} q^\mu}{M_\Theta + M_n} \right] u_n(\mathbf{p}), \quad (7)$$

where the $g_{K^*n\Theta}$ and $f_{K^*n\Theta}$ denote the vector and tensor coupling constants for the $K^*N\Theta$ vertex, respectively. By comparing the Lorentz-structures the strong coupling constants can be determined as

$$g_{K^*n\Theta} = f_{K^*} F_1^{\Theta n}(0), \quad f_{K^*n\Theta} = f_{K^*} F_2^{\Theta n}(0). \quad (8)$$

Using the generalized Goldberger-Treiman relation, we can get the strong coupling constant $g_{Kn\Theta}$ for the $KN\Theta$ vertex as follows:

$$g_{Kn\Theta} = \frac{G_1^{\Theta n}(0) (M_\Theta + M_n)}{2f_K}, \quad (9)$$

where $f_K \approx 1.2f_\pi$ stands for the kaon decay constant.

The form factors $F_1^{n\Theta}(Q^2)$, $F_2^{n\Theta}(Q^2)$ and $G_A^{n\Theta}(Q^2)$ of Eqs. (1) and (2) can be expressed in terms of the matrix elements of the vector and axial-vector currents with their time and space components decomposed in the Θ^+ rest frame as follows:

$$G_E^{n\Theta}(Q^2) = \int \frac{d\Omega_q}{4\pi} \langle \Theta(p') | V^0(0) | n(p) \rangle, \quad (10)$$

$$G_M^{n\Theta}(Q^2) = 3M_n \int \frac{d\Omega_q}{4\pi} \frac{q^i \epsilon^{ik3}}{i\mathbf{q}^2} \langle \Theta(p') | V^k(0) | n(p) \rangle, \quad (11)$$

$$G_A^{n\Theta}(Q^2) = -\frac{3}{2\mathbf{q}^2} \sqrt{\frac{2M_\Theta}{E_\Theta + M_\Theta}} \int \frac{d\Omega_q}{4\pi} \left[\mathbf{q} \times \left(\mathbf{q} \times \langle \Theta(p') | \mathbf{A}(0) | n(p) \rangle \right) \right]_z, \quad (12)$$

where the electromagnetic-like form factors $G_E^{n\Theta}$ and $G_M^{n\Theta}$ are written as

$$G_E^{n\Theta}(Q^2) = \sqrt{\frac{E_n + M_n}{2M_n}} \left[F_1^{n\Theta}(Q^2) - \frac{F_2^{n\Theta}(Q^2)}{M_\Theta + M_n} \frac{\mathbf{q}^2}{E_n + M_n} + F_3^{n\Theta}(Q^2) \frac{q^0}{M_\Theta + M_n} \right], \quad (13)$$

$$G_M^{n\Theta}(Q^2) = \sqrt{\frac{2M_n}{E_n + M_n}} [F_1^{n\Theta}(Q^2) + F_2^{n\Theta}(Q^2)]. \quad (14)$$

Since the second and third parts in Eq. (13) turn out to be very small, we take the following expressions as the vector and tensor coupling constants:

$$g_{K^*n\Theta} = f_{K^*} G_E^{\Theta n}(0), \quad f_{K^*n\Theta} = f_{K^*} (G_E^{\Theta n}(0) - G_M^{\Theta n}(0)). \quad (15)$$

The next step is to evaluate the form factors of Eqs. (10), (11), and (12) within the self-consistent χ QSM. The model is featured by the following effective low-energy partition function with quark fields ψ with the number of colors N_c and the pseudo-Goldstone boson field $U(x)$ in Euclidean space:

$$\mathcal{Z}_{\chi\text{QSM}} = \int \mathcal{D}\psi \mathcal{D}\psi^\dagger \mathcal{D}U \exp \left[- \int d^4x \psi^\dagger iD(U) \psi \right] = \int \mathcal{D}U \exp(-\mathcal{S}_{\text{eff}}[U]), \quad (16)$$

$$\mathcal{S}_{\text{eff}}(U) = -N_c \text{Tr} \ln iD(U), \quad (17)$$

where

$$D(U) = \gamma^4(i\not{\partial} - \hat{m} - MU^{\gamma_5}) = -i\not{\partial}_4 + h(U) - \delta m, \quad (18)$$

$$\delta m = \frac{m_s - \bar{m}}{3} \gamma^4 \mathbf{1}_{3 \times 3} + \frac{\bar{m} - m_s}{\sqrt{3}} \gamma^4 \lambda^8 = M_1 \gamma^4 \mathbf{1}_{3 \times 3} + M_8 \gamma^4 \lambda^8. \quad (19)$$

The current quark mass matrix is defined as $\hat{m} = \text{diag}(\bar{m}, \bar{m}, m_s) = \bar{m} + \delta m$. The \bar{m} designates the average of the up and down current quark masses with isospin symmetry assumed. The M denotes the constituent quark mass of which the best value for the numerical results is $M = 420$ MeV. The pseudo-Goldstone boson field U^{γ_5} is defined as

$$U^{\gamma_5} = \exp(i\gamma_5 \lambda^a \pi^a) = \frac{1 + \gamma_5}{2} U + \frac{1 - \gamma_5}{2} U^\dagger \quad (20)$$

with $U = \exp(i\lambda^a \pi^a)$. For the quantization, we consider here Witten's embedding of SU(2) soliton into SU(3):

$$U_{\text{SU}(3)} = \begin{pmatrix} U_{\text{SU}(2)} & 0 \\ 0 & 1 \end{pmatrix} \quad (21)$$

with the SU(2) hedgehog chiral field

$$U_{\text{SU}(2)} = \exp[i\gamma_5 \hat{\mathbf{n}} \cdot \boldsymbol{\tau} P(r)], \quad (22)$$

Here, the $P(r)$ denotes the profile function of the chiral soliton $U_{\text{SU}(2)}$.

In order to describe the baryonic properties, we first have to derive the profile function. It can be obtained by the following procedure: First, we take the large N_c limit and solve it in the saddle-point approximation, which corresponds at the classical level to finding the profile function $P(r)$ in Eq. (22). Thus, the $P(r)$ can be obtained by solving numerically the classical equation of motion coming from $\delta S_{\text{eff}}/\delta P(r) = 0$, which yields a classical soliton field U_c constructed from a set of single quark energies E_n and corresponding states $|n\rangle$ related to the eigenvalue equation $h(U)|n\rangle = E_n|n\rangle$. However, the classical soliton does not have the quantum number of the baryon states, so that we need to project it to physical baryon states by the semiclassical quantization of the rotational and translational zero modes. Note that

the zero modes can be treated exactly within the functional integral formalism by introducing collective coordinates. Detailed formalisms can be found in Refs. [33, 34]. Considering the rigid rotations and translations of the classical soliton U_c , we can express the soliton field as

$$U(\mathbf{x}, t) = A(t)U_c(\mathbf{x} - \mathbf{z}(t))A^\dagger(t), \quad (23)$$

where $A(t)$ denotes a unitary time-dependent SU(3) collective orientation matrix and $\mathbf{z}(t)$ stands for the time-dependent displacement of the center of mass of the soliton in coordinate space.

In the χ QSM, the baryon state consists of N_c valence quarks expressed as

$$|B(p)\rangle = \lim_{x_4 \rightarrow -\infty} \frac{1}{\sqrt{\mathcal{Z}}} e^{ip_4 x_4} \int d^3 \vec{x} e^{i\vec{p}\cdot\vec{x}} J_B^\dagger(x) |0\rangle \quad (24)$$

with the baryonic current:

$$J_B(x) = \frac{1}{N_c!} \Gamma_B^{\alpha_1 \dots \alpha_{N_c}} \varepsilon^{i_1 \dots i_{N_c}} \psi_{\alpha_1 i_1}(x) \dots \psi_{\alpha_{N_c} i_{N_c}}(x), \quad (25)$$

where $\alpha_1, \dots, \alpha_{N_c}$ and i_1, \dots, i_{N_c} denote the spin-flavor and color indices, respectively. The $\Gamma_B^{\alpha_1 \dots \alpha_{N_c}}$ stands for the projection operator for the corresponding baryon state. Thus, the transition matrix elements in Eqs. (10), (11), and (12) can be written as the following correlation functions:

$$\begin{aligned} \langle B_2(p_2) | \mathcal{J}^{\mu\chi}(0) | B_1(p_1) \rangle &= \frac{1}{\mathcal{Z}} \lim_{T \rightarrow \infty} e^{-ip_2^4 \frac{T}{2} + ip_1^4 \frac{T}{2}} \int d^3 \vec{x}' d^3 \vec{x} e^{i\vec{p}_1 \cdot \vec{x} - i\vec{p}_2 \cdot \vec{x}'} \\ &\times \int \mathcal{D}U \mathcal{D}\psi^\dagger \mathcal{D}\psi J_{B'} \left(\frac{T}{2}, \vec{x}' \right) \mathcal{J}^{\mu\chi}(0) J_B^\dagger \left(-\frac{T}{2}, \vec{x} \right) \exp \left[- \int d^4 x \psi^\dagger iD(U)\psi \right]. \end{aligned} \quad (26)$$

We can solve Eq. (26) in the saddle-point approximation justified in the large N_c limit, taking into account the zero-mode quantization explained before. We consider only the rotational $1/N_c$ corrections and linear m_s corrections. Thus, we expand the quark propagators in Eq. (26) with respect to Ω and δm to the linear order and $\vec{T}_{z(t)}^\dagger T_{z(t)}$ to the zeroth order.

Having carried out a tedious but straightforward calculation (see Refs. [33, 34] for details), we finally can express the baryonic matrix elements in Eqs. (10), (11), and (12) as a Fourier transform in terms of the corresponding quark densities and collective wave-functions of the baryons:

$$\langle B'(p') | \mathcal{J}_\mu^\chi(0) | B(p) \rangle = \int dA \int d^3 z e^{i\mathbf{q}\cdot\mathbf{z}} \Psi_{B'}^*(A) \mathcal{F}_\mu^\chi(\mathbf{z}) \Psi_B(A), \quad (27)$$

where $\Psi(A)$ denote the collective wavefunctions and \mathcal{F}_μ^χ represents the quark densities corresponding to the current operator \mathcal{J}_μ^χ . Using the collective wavefunctions and the quark densities, we immediately obtain the transition vector and axial-vector form factors $G_{E,M,A}^{n\Theta}$ in Eqs. (10), (11), and (12). The corresponding results can be found in Refs. [21, 22], which are summarized in Table I. The vector coupling constant $g_{K^*n\Theta}$ vanishes in SU(3) symmetric case because of the generalized Ademollo-Gatto theorem. Note that even the SU(3) symmetry breaking effects from the Hamiltonian does not contribute to the $g_{K^*n\Theta}$. The value of $g_{K^*n\Theta}$ with SU(3) symmetry breaking comes solely from the wavefunction corrections. The coupling constants for the proton can be obtained easily by considering isospin factors.

Note that there is a sign difference in the coupling constants for the neutron and proton: $g_{K^*n\Theta} = -g_{K^*p\Theta}$ and the same for the $f_{K^*N\Theta}$ [22]. However, as shown in the next section, since the K^* -exchange contribution in the Θ^+ -photoproduction provides a 90° phase difference from others, these sign differences for the neutron and proton targets do not make any difference at all in describing physical observables.

III. AN EFFECTIVE LAGRANGIAN APPROACH

We now proceed to calculate the amplitudes for the reaction of the Θ^+ photoproduction, taking the results of the coupling constants in Section II as numerical inputs. We first define the relevant effective interactions to compute the Θ^+ photoproduction in the Born approximation. Since the coupling constants derived from the χ QSM are for the Θ^+ with positive parity, we assume here the parity of the Θ^+ to be positive.

$$\begin{aligned}
\mathcal{L}_{KN\Theta} &= -ig_{KN\Theta}\bar{\Theta}\gamma_5KN + \text{h.c.}, \\
\mathcal{L}_{K^*N\Theta} &= -g_{K^*N\Theta}\bar{\Theta}\gamma_\mu K^{*\mu}N - \frac{f_{K^*N\Theta}}{M_\Theta + M_N}\bar{\Theta}\sigma_{\mu\nu}\partial^\nu K^{*\mu}N + \text{h.c.}, \\
\mathcal{L}_{\gamma KK} &= ie_K[(\partial^\mu K^\dagger)K - (\partial^\mu K)K^\dagger]A_\mu + \text{h.c.}, \\
\mathcal{L}_{\gamma KK^*} &= g_{\gamma KK^*}\epsilon_{\mu\nu\sigma\rho}(\partial^\mu A^\nu)(\partial^\sigma K^\dagger)K^{*\rho} + \text{h.c.}, \\
\mathcal{L}_{\gamma NN} &= -e_N\bar{N}\left[\gamma_\mu - \frac{\kappa_N}{2M_N}\sigma_{\mu\nu}F^{\mu\nu}\right]N + \text{h.c.}, \\
\mathcal{L}_{\gamma\Theta\Theta} &= -e_\Theta\bar{\Theta}\left[\gamma_\mu - \frac{\kappa_\Theta}{2M_\Theta}\sigma_{\mu\nu}F^{\mu\nu}\right]\Theta + \text{h.c.}, \tag{28}
\end{aligned}$$

where Θ , N , K , and K_μ^* denote the fields of the Θ^+ , the nucleon, the pseudoscalar kaon, and the vector kaon, respectively. The A_μ represents the photon field, whereas the $F_{\mu\nu}$ the antisymmetric electromagnetic field strength. The $g_{\gamma KK^*}$ designates the γKK^* coupling constant that can be determined by using the experimental data for the $K^* \rightarrow K\gamma$ decay, which yields 0.388 GeV^{-1} for the neutral decay and 0.254 GeV^{-1} for the charged one. The e_K , e_N , and e_Θ are unit electric charges for the kaon, nucleon, and Θ^+ , respectively. The κ_N and κ_Θ stand for the anomalous magnetic moments of the nucleon and Θ^+ , respectively. Since the magnetic moment of the Θ^+ is theoretically known to be rather small [6, 35, 36, 37], we take it to be $\kappa_\Theta \approx -0.8$ as in Ref. [26]. The $\sigma_{\mu\nu}$ is a usual antisymmetric spin operator $\sigma_{\mu\nu} = i[\gamma_\mu, \gamma_\nu]/2$. The M_N and M_Θ correspond to the nucleon and Θ^+ masses, and are taken to be 939 MeV and 1540 MeV, respectively.

Having performed straightforward manipulations, we arrive at the following invariant amplitudes for the s - and u -channel contributions, and the K - and K^* -exchange ones in the

$m_s = 0$			$m_s = 180 \text{ MeV}$		
$g_{K^*N\Theta}$	$f_{K^*N\Theta}$	$g_{KN\Theta}$	$g_{K^*N\Theta}$	$f_{K^*N\Theta}$	$g_{KN\Theta}$
0	2.91	1.41	0.81	0.84	0.83

TABLE I: The results for the $K^*N\Theta$ and $KN\Theta^+$ coupling constants at $Q^2 = 0$ with and without m_s corrections. The constituent quark mass M is taken to be $M = 420 \text{ MeV}$.

t -channel as follows:

$$\begin{aligned}
i\mathcal{M}_s &= -g_{KN\Theta}\bar{u}(p_2) \left[e_N\gamma_5 \frac{F_c(\not{p}_1 + M_N) + F_s\not{k}_1}{s - M_N^2} \not{\epsilon} - \frac{e_Q\kappa_N}{2M_N}\gamma_5 \frac{F_s(\not{k}_1 + \not{p}_1 + M_N)}{s - M_N^2} \not{\epsilon}\not{k}_1 \right] u(p_1), \\
i\mathcal{M}_u &= -g_{KN\Theta}\bar{u}(p_2) \left[e_\Theta\not{\epsilon} \frac{F_c(\not{p}_2 + M_\Theta) - F_u\not{k}_1}{u - M_\Theta^2} \gamma_5 - \frac{e_Q\kappa_\Theta}{2M_\Theta}\not{\epsilon}\not{k}_1 \frac{F_u(\not{p}_2 - \not{k}_1 + M_\Theta)}{u - M_\Theta^2} \gamma_5 \right] u(p_1), \\
i\mathcal{M}_t^K &= 2e_K g_{KN\Theta}\bar{u}(p_2)\gamma_5 \frac{(k_2 \cdot \epsilon)}{t - M_K^2} u(p_1) F_c, \\
\mathcal{M}_t^{K^*} &= ig_\gamma g_{KK^*}\epsilon_{\mu\nu\sigma\rho}\bar{u}(p_2) \left[g_{K^*N\Theta}(t) \frac{k_1^\mu \epsilon^\nu k_2^\sigma \gamma^\rho}{t - M_{K^*}^2} \right. \\
&\quad \left. - \frac{f_{K^*N\Theta}(t)}{2(M_N + M_\Theta)} \frac{k_1^\mu \epsilon^\nu k_2^\sigma \gamma^\rho \not{q}_t - \not{q}_t k_1^\mu \epsilon^\nu k_2^\sigma \gamma^\rho}{t - M_{K^*}^2} \right] u(p_1) F_v^{1/2}, \quad (29)
\end{aligned}$$

where \bar{u} and u are the Dirac spinors of Θ^+ and the nucleon. The four momenta p_1 , p_2 , k_1 , and k_2 stand for those of the nucleon, the Θ^+ , the photon, and the kaon, respectively. The s , u and t represent the Mandelstam variables. Note that in the case of the process $\gamma p \rightarrow \bar{K}^0\Theta^+$, there is no contribution from the K -exchange contribution. Moreover, the K^* -exchange contribution gives a 90° phase difference from others as mentioned previously.

The form factors as functions of the Mandelstam variables are defined as follows [27, 28]:

$$F_{s,u,t} = \frac{\Lambda^4}{\Lambda^4 + [(s, u, t) - M_{s,u,t}^2]^2}, \quad F_v = \frac{\Lambda^4}{\Lambda^4 + (t - M_{K^*}^2)^2}, \quad (30)$$

where the four-dimensional cutoff mass Λ is chosen to be 650 MeV which is compatible with those used in the $\Lambda(1520)$ [29] and $\Lambda(1116)$ [30] photoproductions. The common overall form factor F_c is written as follows:

$$F_c(s, t, u) = 1 - (1 - F_s)(1 - F_u)(1 - F_t), \quad (31)$$

which satisfies the on-shell condition and crossing symmetry. We note that this form-factor scheme preserves the Ward-Takahashi identity explicitly.

As for the coupling constants $g_{K^*N\Theta}$, $f_{K^*N\Theta}$, and $g_{KN\Theta}$, we take the forms of Eq. (15) with the results of the χ QSM. The corresponding form factors from the χ QSM can be parameterized as follows [21]:

$$G_E^{m\Theta}(t) = G_E^0 \left[\frac{\alpha_E \Lambda_E^2}{\alpha_E \Lambda_E^2 - t} \right]^\alpha + b, \quad G_M^{n\Theta}(t) = G_M^0 \left[\frac{\alpha_M \Lambda_M^2}{\alpha_M \Lambda_M^2 - t} \right]^\alpha, \quad (32)$$

where fitting parameters $\alpha_{E,M}$, $\Lambda_{E,M}$, and b are listed in Table II. These parameters are determined by using the results with the strange quark mass $m_s = 180$ MeV and the constituent quark mass $M = 420$ MeV.

IV. NUMERICAL RESULTS AND DISCUSSION

We are now in a position to discuss the results of the present work. As mentioned previously, we assume that the Θ^+ baryon has the spin-parity quantum number, $1/2^+$. In

the left panel of Fig. 1, each contribution to the total cross section of the $\gamma n \rightarrow K^- \Theta^+$ reaction is drawn as a function of the photon energy E_γ . As shown there in Fig. 1, the K -exchange contribution is the most dominant one, whereas the second dominant one comes from the K^* -exchange one. The K^* -exchange contribution is, however, the most dominant one near the threshold up to around 1.8 GeV, because of which the total cross section is raised drastically near the threshold. The u -channel contribution is rather small and the s -channel is almost negligible due to the present form-factor scheme that suppresses these channels. The K -exchange contribution shows rather strong dependence on the photon energy E_γ . As the E_γ increases, it starts to get enhanced.

The right panel of Fig. 1 depicts each contribution to the differential cross section of the $\gamma n \rightarrow K^- \Theta^+$ reaction. The tendency of each contribution is in general similar to the case of the total cross section, *i.e.* the K -exchange contribution turns out to be the dominant one, as it should be. Moreover, it has a large bump structure in the forward direction. Beginning from the backward direction, it is getting increased slowly. In the forward direction, it starts to increase drastically till around $\cos \theta_{\text{cm}} \approx 0.75$ and falls down sharply, which makes the K -exchange contribution have the bump structure. The K^* -exchange contribution is also larger in the forward direction than in the backward direction. The u -channel contributes mainly to the backward direction as expected. Summing up all contributions, we can easily see that the differential cross section is much more enhanced in the forward direction.

A. Effects of the K^* exchange

Since the present work is mainly interested in the effects of the K^* -exchange contribution, we now examine the features of the K^* -exchange contribution to various observable in detail. In the two-upper panels of Fig. 2, the total cross sections of the $\gamma n \rightarrow K^- \Theta^+$ and $\gamma p \rightarrow \bar{K}^0 \Theta^+$ reactions are drawn in the left and right panels, respectively. The K^* -exchange contribution turns out to be almost 30% to the total cross section for the neutron target. On the other hand, it is almost everything for the proton target. It can be easily understood from the fact that for the $\gamma p \rightarrow \bar{K}^0 \Theta^+$ reaction there is no K -exchange contribution that is dominant in the neutron channel. Comparing the total cross sections for the neutron target with the proton one, we find that that for the neutron one is about 30% larger than that for the proton one, although they are qualitatively in a similar order $\lesssim 1$ nb.

In the two lower panels of Fig. 2, we show the differential cross sections for the $\gamma n \rightarrow K^- \Theta^+$ and $\gamma p \rightarrow \bar{K}^0 \Theta^+$ reactions with and without the K^* -exchange contribution for three different photon energies 2.1 GeV, 2.2 GeV, and 2.3 GeV, respectively, in the left and right panels. According to the K - and K^* -exchange contributions, one can observe the bump structures in the region $\lesssim 60^\circ$ for both the neutron and proton target cases. As in the case of the total cross sections, while the K^* -exchange contribution makes the differential cross section about 10% enhanced for the neutron target, its effects are remarkably large for the

$G_E^{n\Theta}(t)$				$G_M^{n\Theta}(t)$		
G_E^0	α_E	Λ_E	b	G_M^0	α_M	Λ_M
0.182	9.01	0.402	-0.04	0.286	0.851	0.559

TABLE II: Relevant parameters for the electric and magnetic vector-transition form factors derived in Eq. (32).

proton target. As the photon energy increases, the differential cross sections also increase consistently, as expected.

In the two upper panels of Fig. 3, we represent the differential cross section as a function of the momentum transfer t . The general tendency is very similar to that of the differential cross sections shown in Fig. 2. It is worth mentioning that the best way to examine the effects of the K^* -exchange contribution is to investigate the photon beam asymmetry, since the K^* meson is a vector meson which manifests magnetic meson-baryon coupling behavior in the present photoproduction process. The photon beam asymmetry is defined as

$$\Sigma = \left[\frac{d\sigma}{d\Omega_{\perp}} - \frac{d\sigma}{d\Omega_{\parallel}} \right] \times \left[\frac{d\sigma}{d\Omega_{\perp}} + \frac{d\sigma}{d\Omega_{\parallel}} \right]^{-1}, \quad (33)$$

where the subscript \perp (\parallel) denotes that the polarization vector of the incident photon is perpendicular (parallel) to the reaction plane. In the two-lower panels of Fig. 3 draws the photon beam asymmetries for the $\gamma n \rightarrow K^-\Theta^+$ and $\gamma p \rightarrow \bar{K}^0\Theta^+$ reactions in the left and right panels, respectively. When we switch off the K^* -exchange contribution, the photon beam asymmetry for the neutron target, starting from the backward direction, is brought down drastically and reaches down to almost $\Sigma = -1$ at around $\theta_{\text{cm}} = 90^\circ$, due to the electric meson-baryon coupling of the dominant K -exchange contribution. However, when we turn on the K^* -exchange one, the photon beam asymmetry decreases mildly from the backward direction to the forward direction, and then it increases sharply to $\Sigma = 0$. On the whole, the photon beam asymmetry is negative for the neutron target.

When it comes to the proton target, the K^* -exchange contribution shows profound effects on the photon beam asymmetry. While the photon beam asymmetry becomes negative without the K^* -exchange contribution, it turns into being positive with it in all the regions. With the K^* -exchange contribution switched on, the photon beam asymmetry starts to increase from the backward direction to the forward direction, and it goes down from around $\cos\theta_{\text{cm}} = 0.5$.

B. Effects of explicit SU(3) symmetry breaking

In Sec. II, it was mentioned that the vector coupling constant $g_{K^*N\Theta}$ vanishes in the SU(3) symmetric case due to the generalized Ademollo-Gatto theorem. Moreover, the tensor coupling constant $f_{K^*N\Theta}$ is also very sensitive to SU(3) symmetry breaking as shown in Table I. Thus, it is of great interest to see the effects of SU(3) symmetry breaking on the Θ^+ photoproduction. In Fig. 4, we show the total (upper), differential (middle) cross sections, and photon beam asymmetries (lower) for the neutron and proton targets in the left and right panels, respectively. Although the values of the vector and tensor couplings for the $K^*N\Theta$ vertex are rather sensitive to the effects of SU(3) symmetry breaking, all the results indicate that SU(3) symmetry breaking does not play any significant role in describing the Θ^+ photoproduction. The reason can be found in the fact that while the tensor coupling constant $f_{K^*N\Theta}$ is almost three times reduced by SU(3) symmetry breaking, the vector coupling constant $g_{K^*N\Theta}$ comes solely from the wavefunction corrections that are also a part of the SU(3) symmetry breaking effects. Thus, the finite value of the $g_{K^*N\Theta}$ makes up for the reduction of the $f_{K^*N\Theta}$, so that the effects of SU(3) symmetry breaking turn out to be rather small.

V. SUMMARY AND CONCLUSION

In the present work, we have investigated the Θ^+ photoproduction, taking the new results of the chiral quark-soliton model [21, 22] into account. We first have briefly reviewed the formalism of the chiral quark-soliton model for deriving the coupling constants and form factors for the $K^*N\Theta$ and $KN\Theta$ vertices. We made use of these coupling constants and form factors as numerical inputs for calculating the $\gamma n \rightarrow K^-\Theta^+$ and $\gamma p \rightarrow \bar{K}^0\Theta^+$ scattering processes.

We have examined the effects of each contribution to the total and differential cross sections. It turned out that the K -exchange contribution is the most dominant one except for the near-threshold region in which the K^* -exchange contributes mainly. The differential cross section has a large bump structure in the forward direction, which is obviously due to the K - and K^* -exchange contributions.

Since it is of great importance to understand how the K^* -exchange contribution plays a role in the Θ^+ photoproduction, we thoroughly have studied the effects of the K^* -exchange contribution in various observables for the $\gamma n \rightarrow K^-\Theta^+$ and $\gamma p \rightarrow \bar{K}^0\Theta^+$ reactions. It turned out that the K^* -exchange contribution is in general the most dominant one in the $\gamma p \rightarrow \bar{K}^0\Theta^+$ reaction, since there is no K -exchange contribution for the proton target. The K^* -exchange contribution to the $\gamma n \rightarrow K^-\Theta^+$ reaction is in general about 30% but to the $\gamma p \rightarrow \bar{K}^0\Theta^+$ reaction it is almost everything, since the K -exchange contribution is absent in this case. In order to see the effects of the K^* -exchange contribution, we also calculated the photon beam asymmetries. It was shown that with the K^* -exchange contribution the photon beam asymmetries are very different from those without the K^* -exchange contribution. In particular, the photon beam asymmetry for the proton target is changed from the negative sign to the positive with K^* -exchange turned on.

The effects of SU(3) symmetry breaking are remarkable on the coupling constants for the $K^*N\Theta$ vertex. The vector coupling constant $g_{K^*N\Theta}$ vanishes without SU(3) symmetry breaking, *i.e.* $g_{K^*N\Theta} = 0$. The tensor coupling constant becomes $f_{K^*N\Theta} = 2.91$ that is by no means small. When we switched on SU(3) symmetry breaking, the vector-coupling constant became finite because of the wavefunction corrections. Moreover, the tensor coupling constant is reduced about by a factor of three. Thus, one may see this large changes in the coupling constants in the observables. However, it was found that the effects of SU(3) symmetry breaking were rather small in all observables we calculated in the present work. It indicates that the finite value of the vector coupling constant makes up for the reduction of the tensor coupling constant. Thus, the effects of SU(3) symmetry breaking altogether turn out to be small.

Recent KEK and LEPS experiments [12, 17] have drawn a conclusion that the $K^*N\Theta$ coupling constants must be small, since the total cross sections turned out to be tiny for the proton target, being rather different from the present results. In contrast, the present results for the neutron target is compatible with the experimental data [17]. In order to pin down this inconsistency between the theory and experiments, it is of great importance to have more high-statistics data for various physical observable for the Θ^+ -production experiment [38].

Acknowledgment

The authors would like to thank J. K. Ahn, A. Hosaka, and T. Nakano for fruitful discussions. They especially are grateful to T. Ledwig for discussing the results from the chiral

quark-soliton model. The work of S.i.N. is partially supported by the Grant for Scientific Research (Priority Area No.17070002 and No.20028005) from the Ministry of Education, Culture, Science and Technology (MEXT) of Japan. The work of H.Ch.K. is supported by the Korea Research Foundation Grant funded by the Korean Government(MOEHRD) (KRF-2006-312-C00507). This work was done under the Yukawa International Program for Quark-Hadron Sciences. The numerical calculations were carried out on MIHO at RCNP in Osaka University and YISUN at YITP in Kyoto University.

-
- [1] T. Nakano *et al.* [LEPS Collaboration], Phys. Rev. Lett. **91**, 012002 (2003).
 - [2] D. Diakonov, V. Petrov, and M. V. Polyakov, Z. Phys. A **359**, 305 (1997).
 - [3] M. Praszalowicz, Phys. Lett. B **575**, 234 (2003).
 - [4] C. Amsler *et al.*, Phys. Lett. B **667**, 1 (2008).
 - [5] K. H. Hicks, Prog. Part. Nucl. Phys. **55**, 647 (2005) and references therein.
 - [6] K. Goeke *et al.*, Prog. Part. Nucl. Phys. **55**, 350 (2005).
 - [7] M. Battaglieri *et al.* [CLAS Collaboration], Phys. Rev. Lett. **96**, 042001 (2006).
 - [8] B. McKinnon *et al.* [CLAS Collaboration], Phys. Rev. Lett. **96**, 212001 (2006).
 - [9] S. Niccolai *et al.* [CLAS Collaboration], Phys. Rev. Lett. **97**, 032001 (2006).
 - [10] R. De Vita *et al.* [CLAS Collaboration], Phys. Rev. D **74**, 032001 (2006).
 - [11] K. Miwa *et al.* [KEK-PS E522 Collaboration], Phys. Lett. B **635**, 72 (2006).
 - [12] K. Miwa *et al.*, Phys. Rev. C **77**, 045203 (2008).
 - [13] V. V. Barmin *et al.* [DIANA Collaboration], Phys. Atom. Nucl. **70**, 35 (2007).
 - [14] V. V. Barmin *et al.* [DIANA Collaboration], Phys. Atom. Nucl. **66**, 1715 (2003).
 - [15] A. Aleev *et al.* [SVD Collaboration], hep-ex/0509033.
 - [16] A. Aleev *et al.* [SVD Collaboration], arXiv:0803.3313 [hep-ex].
 - [17] T. Nakano *et al.* [LEPS collaboration], arXiv:0812.1035 [nucl-ex].
 - [18] D. Diakonov, Prog. Theor. Phys. Suppl. **168**, 1 (2007).
 - [19] H. Kwee, M. Guidal, M. V. Polyakov and M. Vanderhaeghen, Phys. Rev. D **72**, 054012 (2005).
 - [20] Y. Azimov, V. Kuznetsov, M. V. Polyakov and I. Strakovsky, Phys. Rev. D **75**, 054014 (2007).
 - [21] T. Ledwig, H. -Ch. Kim and K. Goeke, Nucl. Phys. A **811**, 353 (2008).
 - [22] T. Ledwig, H. -Ch. Kim and K. Goeke, Phys. Rev. D **78**, 054005 (2008).
 - [23] S. i. Nam, A. Hosaka and H. -Ch. Kim, Phys. Lett. B **579**, 43 (2004).
 - [24] W. Liu and C. M. Ko, Nucl. Phys. A **741**, 215 (2004).
 - [25] Y. s. Oh, H. c. Kim and S. H. Lee, Phys. Rev. D **69**, 014009 (2004).
 - [26] S. i. Nam, A. Hosaka and H. -Ch. Kim, J. Korean Phys. Soc. **49**, 1928 (2006).
 - [27] H. Haberzettl, C. Bennhold, T. Mart and T. Feuster, Phys. Rev. C **58**, 40 (1998).
 - [28] R. M. Davidson and R. Workman, Phys. Rev. C **63**, 025210 (2001).
 - [29] S. i. Nam, A. Hosaka and H. -Ch. Kim, Phys. Rev. D **71**, 114012 (2005).
 - [30] S. Ozaki, H. Nagahiro and A. Hosaka, Phys. Lett. B **665**, 178 (2008).
 - [31] J. J. Sakurai, Annals Phys. **11**, 1 (1960); "Currents and Mesons",
(The University of Chicago Press, Chicago, 1969).
 - [32] R. P. Feynman, "Photon-Hadron Interactions," (W.A. Benjamin, Inc. Reading, MA, 1972).
 - [33] C. V. Christov *et al.*, Prog. Part. Nucl. Phys. **37**, 91 (1996).
 - [34] H. -Ch. Kim, A. Blotz, M.V. Polyakov and K. Goeke, Phys. Rev. D **53**, 4013 (1996).
 - [35] H. -Ch. Kim and M. Praszalowicz, Phys. Lett. B **585**, 99 (2004).

- [36] Gh. S. Yang, H. -Ch. Kim, M. Praszalowicz and K. Goetze, Phys. Rev. D **70**, 114002 (2004).
- [37] P. Z. Huang, W. Z. Deng, X. L. Chen and S. L. Zhu, Phys. Rev. D **69**, 074004 (2004).
- [38] Private communications with T. Nakano and H. Kohri for the LEPS collaboration at SPring-8.

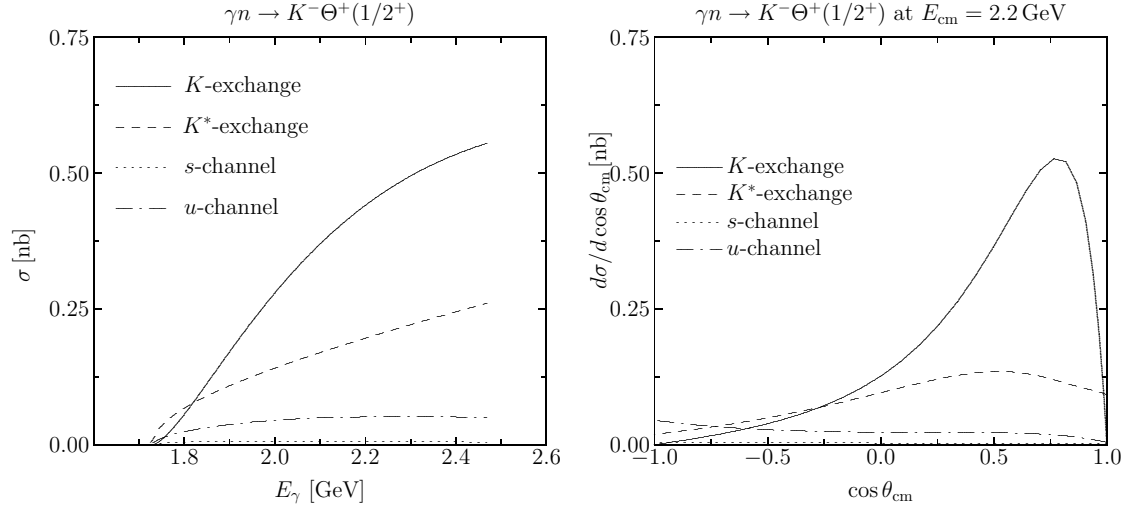


FIG. 1: Each contribution to the total and differential cross sections for the $\gamma n \rightarrow K^- \Theta^+$ reaction. The total cross section is drawn in the left panel, while the differential cross section for the photon energy $E_\gamma = 2.2 \text{ GeV}$ is in the right panel. The solid curve stands for the K -exchange contribution, the dashed one for the K^* -exchange, the dotted curve for the s -channel, and the dash-dotted one for the u -channel contributions.

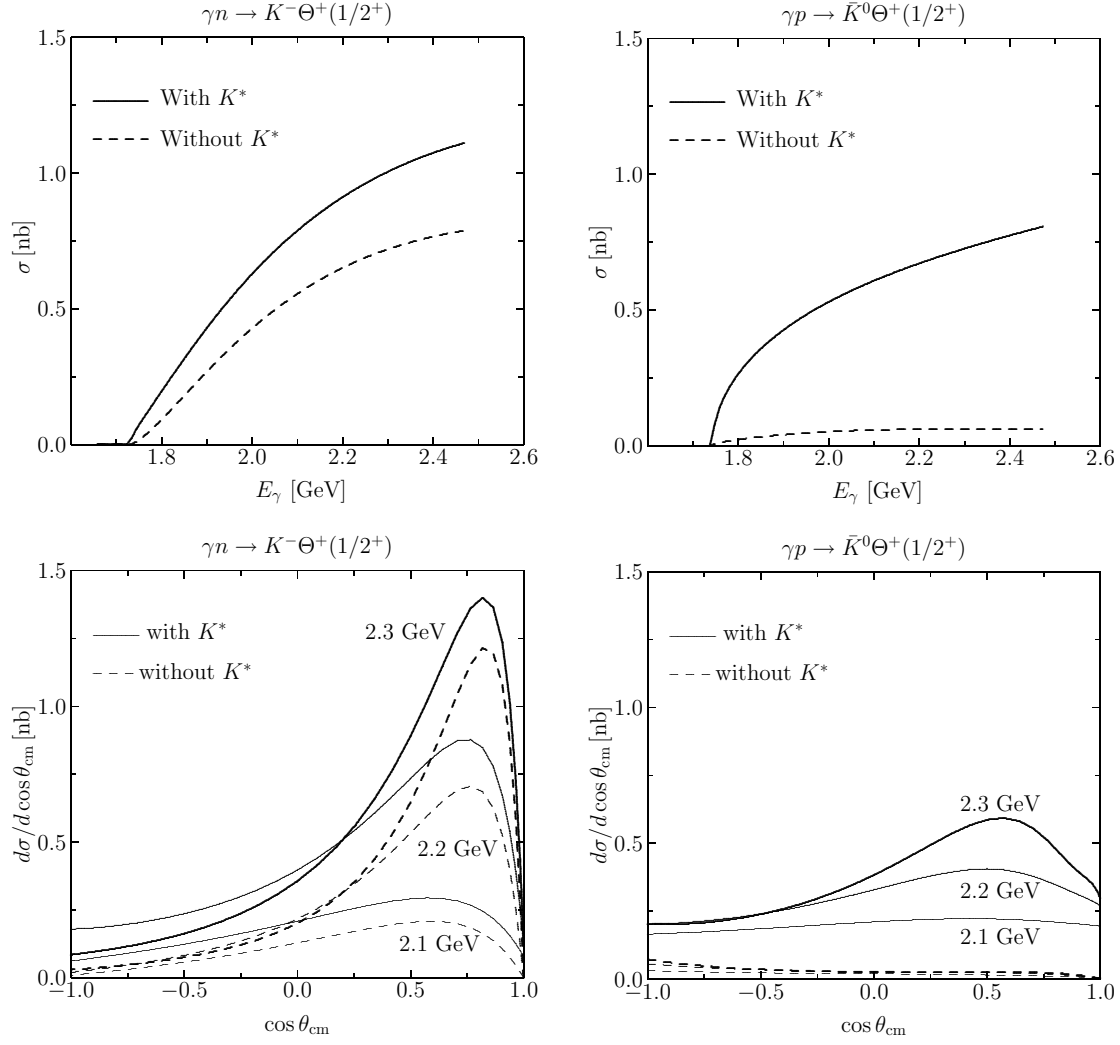


FIG. 2: Effects of the K^* -exchange on the total (upper panels) and differential (lower panels) cross sections. The left panels represent those for the $\gamma n \rightarrow K^- \Theta^+$ reaction, while the right panels those for the $\gamma p \rightarrow \bar{K}^0 \Theta^+$. The solid curves indicate those with all contributions, whereas the dashed one those without the K^* -exchange. The differential cross sections are drawn for three different photon energies E_γ , 2.1 GeV, 2.2 GeV, and 2.3 GeV.

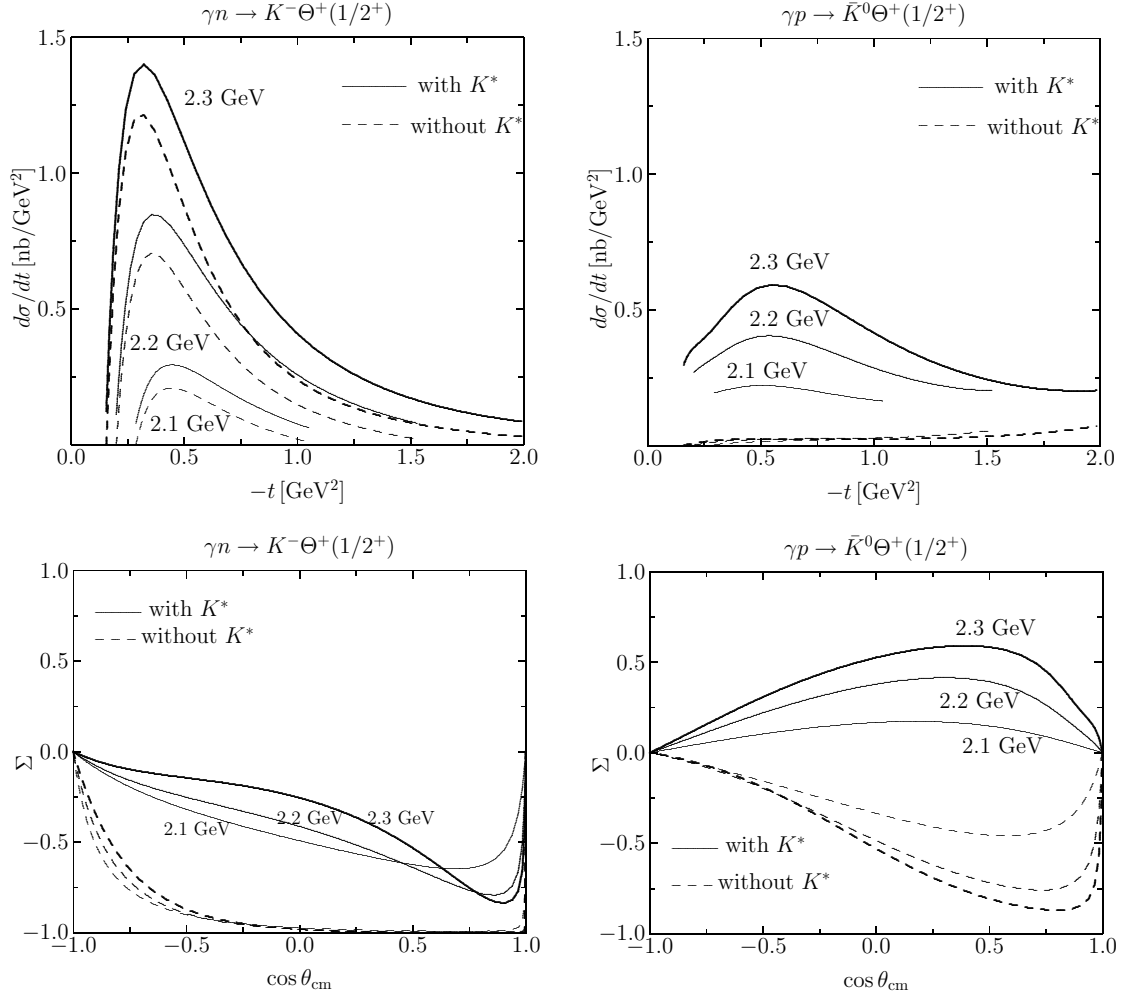


FIG. 3: Effects of the K^* -exchange on the t -dependences ($d\sigma/dt$, upper panels) and the photon-beam asymmetries (Σ , lower panels). The left panels represent those for the $\gamma n \rightarrow K^- \Theta^+$ reaction, while the right panels those for the $\gamma p \rightarrow \bar{K}^0 \Theta^+$. The solid curve indicates the case with all contributions, whereas the dashed one that without the K^* -exchange. The curves are drawn for three different photon energies E_γ , 2.1 GeV, 2.2 GeV, and 2.3 GeV.

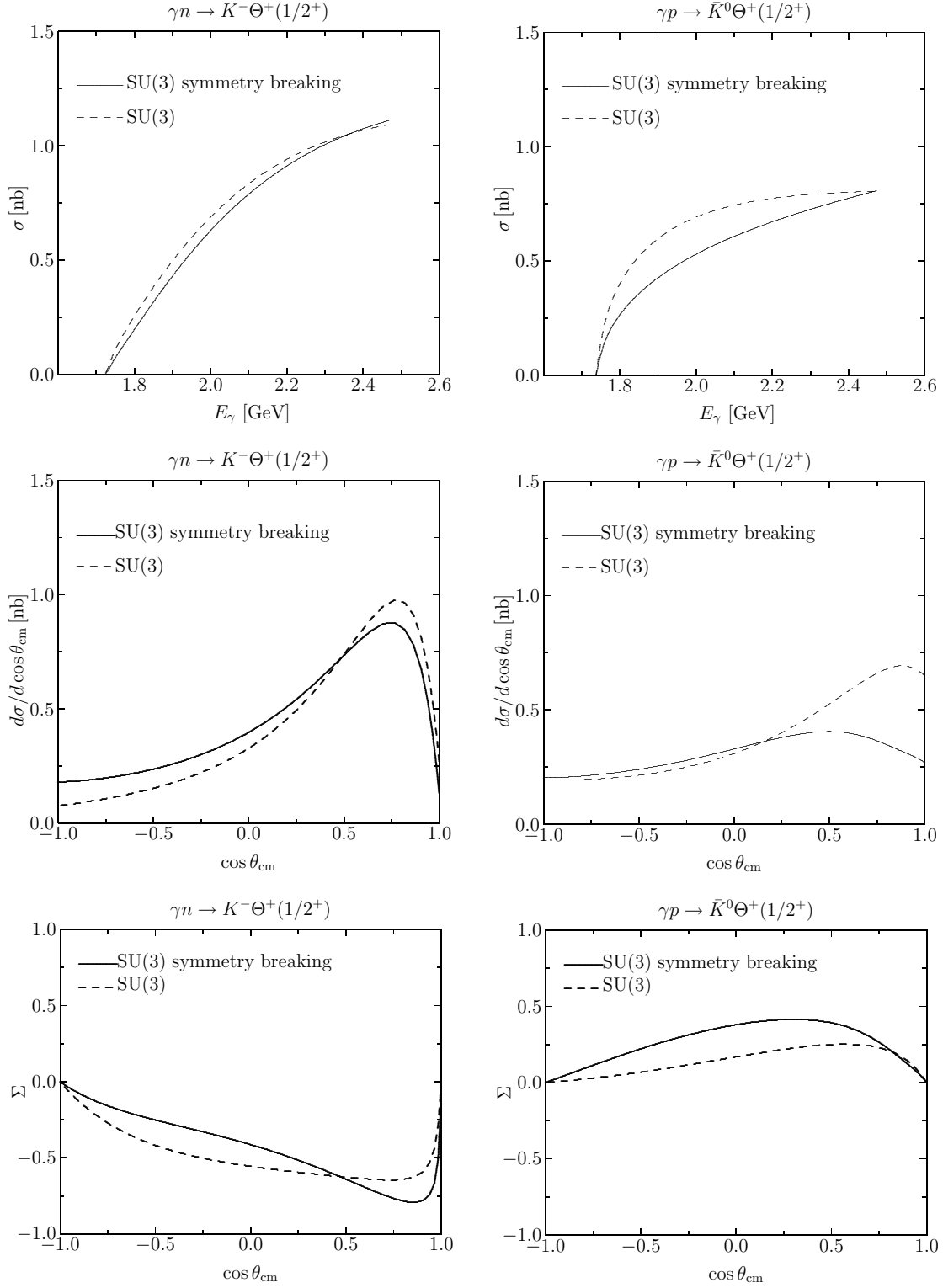


FIG. 4: Effects of SU(3) symmetry breaking on the total (σ , upper), differential ($d\sigma/d\cos\theta_{\text{cm}}$, middle) cross sections, and photon-beam asymmetries (Σ , lower) as functions of the photon energy E_γ . The left panels represent those for the $\gamma n \rightarrow K^- \Theta^+$ reaction, while the right panels those for the $\gamma p \rightarrow \bar{K}^0 \Theta^+$. The solid curve draws the total cross section with SU(3) symmetry breaking, whereas the dashed one depicts that without it. The curves are drawn for three different photon energies E_γ , 2.1 GeV, 2.2 GeV, and 2.3 GeV. 17